Design and Synthesis of Novel Indolinone Aurora B Kinase Inhibitors Based on Fragment-Based Drug Discovery (FBDD)

Baoxing Xie
Xinjiang Technical Institute of Physics and Chemistry, Chinese Academy of Sciences
Miaomiao Shi
Xinjiang Technical Institute of Physics and Chemistry, Chinese Academy of Sciences
Dan Tang
Xinjiang Technical Institute of Physics and Chemistry, Chinese Academy of Sciences
Shan Yang
Xinjiang Technical Institute of Physics and Chemistry, Chinese Academy of Sciences
Yan Zeng
Xinjiang Institute of Engineering
Lifei Nie
Xinjiang Technical Institute of Physics and Chemistry, Chinese Academy of Sciences
Chao Niu
niuchao@ms.xjb.ac.cn

Xinjiang Technical Institute of Physics and Chemistry, Chinese Academy of Sciences

Research Article

Keywords: Aurora B, Tumor, Indolinone derivatives, FBDD, Pharmacophore

Posted Date: July 21st, 2025

DOI: https://doi.org/10.21203/rs.3.rs-7130864/v1

Additional Declarations: No competing interests reported.

Version of Record: A version of this preprint was published at Molecular Diversity on September 10th, 2025. See the published version at https://doi.org/10.1007/s11030-025-11353-w.

Abstract

Aurora kinases are a group of serine/threonine kinases essential for cell mitosis, comprising Aurora A, B, and C. However, the Aurora B is overexpressed in multiple tumors and the aurone has been proved to exhibit potent inhibitory activity against Aurora B kinase by our group. The indolinone was considered as aurone scaffold hopping analog, and the indolinone-based Aurora B inhibitors library (3577 Mols) was performed by FBDD strategy. After pharmacophore model and molecular docking, the candidate molecules were identified and synthesized via Knoevenagel, Suzuki-Miyaura reaction. The compounds **3-17a**, **3-17d** and **3-17k** especially inhibited Aurora B in the nanomolar range (IC_{50} = 1.100, 1.518 and 0.8911 nM, respectively), with a negligible activity against Aurora A. Notably, the most potent **3-17k** demonstrated the strongest antiproliferative activity against HGC27 (IC_{50} = 2.05 μM) and HT-29 (IC_{50} = 2.07 μM) cell line, as well as Aurora B over-expression cells, including OVCAR8 (IC_{50} = 3.02 μM), T24 (IC_{50} = 10.21 μM), NCIH1299 (IC_{50} = 7.32 μM) and SW480 (IC_{50} = 4.45 μM), while maintaining low cytotoxicity in normal human cells (GES-1 and NCM460), representing >50-fold selectivity. Additionally, molecular dynamics simulation were conducted to explore the binding interactions between **3-17k** and Aurora B (PDB: 5EYK), revealing favorable binding free energy (-33.34 kcal·mol-1). In summary, Compound **3-17k** merits further investigation to discover a potential therapeutic candidate against cancer.

1. Introduction

Aurones, a subclass of flavonoids [1], are characterized by a benzofuranone core linked to a phenyl ring through an exocyclic carbon-carbon double bond [2], have been demonstrated to possess diverse biological activities, including antitumor, antibacterial, anti-inflammatory, and antioxidant properties [4–8]. Our group successfully isolated a aurone **HJ-1**, from *Coreopsis tinctoria*, which exhibited moderate inhibitory activity against Human liver cancer cells (Fig. 1).

Aurora B kinase is a critical serine/threonine kinase and a core component of the Chromosome Passenger Complex (CPC), playing essential roles in chromosome segregation, spindle assembly checkpoint (SAC) regulation, and cytokinesis [9]. Unlike Aurora A and C, Aurora B primarily localizes to centromeres and kinetochores during early mitosis, ensuring proper microtubule-kinetochore attachments and correcting erroneous attachments to maintain mitotic fidelity [10]. Aurora B kinase plays a multifaceted role in cancer development and progression through its essential mitotic functions [11]. Aberrant overexpression of Aurora B has been documented in various malignancies, including breast, colorectal, ovarian, and hematological cancers [12], where it contributes to tumorigenesis through several mechanisms [13, 14].

Currently, at least 18 Aurora B inhibitors are in preclinical or clinical studies (Fig. 2) [15]. As a novel antitumor target, Aurora B has been relatively understudied, and research on aurone-based Aurora B inhibitors is even rarer.

In our group, structural derivatization on **HJ-1** yielded multiple analogs and several of them demonstrated potent inhibitory rate against Aurora B kinase with a high selectivity at a concentration of 1 μM (Fig. 3). However, challenges such as poor bioavailability and suboptimal anticancer efficacy of aurone remain to be addressed. Inspired by Hesperadin and BI-847325 (Fig. 2), the privileged indolone scaffold was obtained through scaffold hopping (Fig. 4).

2. Results and discussion

2.1 Compounds design

Fragment-based drug discovery (FBDD) [16] has emerged as a powerful tool for identifying novel therapeutic agents. The application of AIDD significantly enhances drug discovery efficiency. Our FBDD strategy involves (**Figure S1**):
1. A Enumeration library of Aurora B inhibitor (3577 Mols) was constructed by recombining hydrophobic and hydrophilic fragments from literatures via *Recap* and BRICS [17].

2. Constructing a ligand-receptor complex-based pharmacophore (CBP) model (**Table S1**) to screen our Aurora B kinase inhibitors (**Figure S2**, **S3**) [18], followed by molecular docking to find the top 20 hit compounds.

3. The hits were screened according to synthetic accessibility and “Lipinski's rule of five" to identify the candidate compound.

Based on this, the scaffold **3** (Fig. 5) was found and 15 novel ccompounds were synthesized.

2.2 Chemistry

The target compounds were deconstructed into three components: hydrophobic fragments, scaffold, and hydrophilic fragments (Fig. 5). We employed a modular assembly approach for faster and more efficient compound synthesis.

Starting with 6-amino-2-indolinone (**3 – 1**), nucleophilic addition with various 3-substituted isocyanatobenzenes (**3 – 2**) yielded intermediate **3–3** (**Part A**). From 5-formyl-2,4-dimethyl-1*H*-pyrrole-3-carboxylic acid (**3–4**), amidation with compound **3–5** (either 1-(2-aminoethyl)pyrrolidine or *N*, *N*-diethylethylenediamine) under EDC·HCl and HOBt activation afforded intermediate **3–6** (**Part B**). Condensation of 3-bromo-1*H*-pyrazol-5-amine (**3–7**) with propionyl chloride (**3–8**) gave **3–9**, which then underwent a Suzuki coupling with **3–10** to construct intermediate **3–11 (Part C)**. Nucleophilic substitution of 1*H*-pyrazole-4-carbaldehyde (**3–12**) with (2-bromoethoxy)(tert-butyl)dimethylsilane (**3–13**) produced **3–14** (**Part D**). Similarly in **Part E**, using 6-amino-2-indolinone (**3 – 1**) as the starting material, nucleophilic substitution with 2-chloro-*N*-cyclopropylacetamide (**3–15**) yielded intermediate **3–16** (Scheme 1).

For the final compounds (**F**, **G**, **H**, and **I**). The intermediates obtained above (**3–3** or **3–11** or **3–16** between **3–6** or **3–14**) were connected via aldol condensation or Knoevenagel condensation

to furnish the target compound **3–17** [19]. Control compound **3–19** was synthesized via aldol condensation between 2-indolinone (**3–18**) and **3-6b** (Scheme 2).

Moreover, we systematically optimized the Suzuki coupling conditions and established the optimal reaction parameters as: **3–9** (1.0 mol), **3–10** (1.20 mmol), K_2CO_3 (3.0 mmol), $Pd(PPh_3)_4$ (0.05 mmol) in 5.0 mL 1,4-dioxane and 1.0 mL H_2O, was refluxed at 105 ^oC for 18 h and afforded **3–11** with a 70% yield (**Table S2**).

2.3 SAR

The structure–activity relationship (SAR) was concentrated on the R_1 group on the phenyl ring of compound **3-17a** – 3**-17k**. As shown in Fig. 6, the hydrophobic phenylurea moiety demonstrates essential pharmacological importance, since the activity significantly decreases when replaced with amide (**3-17l**) or pyrazole amide (**3-17n**) groups. And complete removal of hydrophobic fragments (**3–19**) resulted in total activity abolition. The ring-opening of the hydrophilic tetrahydropyrrole fragment

Table 1
The cytotoxicity of Aurora B inhibitors against tumor cells versus normal cells

	HELA IC_{50} (μM)	HGC27 IC_{50} (μM)	HT-29 IC_{50} (μM)	MCF7 IC_{50} (μM)	GES-1 IC_{50} (μM)	SI	NCM460 IC_{50} (μM)	SI
3-17a	*NI*[a]	4.04	2.70	*NI*	31.17	7.76	22.25	8.24
3-17c	*NI*	14.82	*NI*	*NI*	_[b]		-	
3-17d	*NI*	2.82	2.51	*NI*	98.04	34.77	64.66	25.76
3-17f	*NI*	6.11	18.27	*NI*	-		-	
3-17h	*NI*	11.71	*NI*	*NI*	-		-	
3-17i	*NI*	4.52	*NI*	*NI*	-		-	
3-17j	*NI*	14.65	6.05	*NI*	-		-	
3-17k	*NI*	2.05	2.07	*NI*	201.50	98.29	160.37	77.47
3-17m	*NI*	22.56	20.87	*NI*	-		-	
Hesperadin	*NI*	4.38	7.32	8.96	56.34	12.86	34.87	4.76
DOX	0.9	0.32	0.12	0.8	8.59 (nM)		0.6 (nM)	

[a] NI: IC_{50} > 50 μM; [b] Not test.

showed negligible impact on biological activity (**3-17a** and **3-17e**). The activity was enhanced when the benzene ring bears both halogen and electron-donating groups. When R_1 = Cl (**3-17a**), -CH_3 (**3-17d**) and F (**3-17k**), all three compounds exhibited superior activity against Aurora with IC_{50} values of 1.100, 1.518 and 0.8911 nM respectively, which were comparable to that of the positive control CCT241736 (IC_{50} = 2.137 nM), an orally bioavailable dual FLT3 and Aurora kinase inhibitor. Meanwhile, we also tested the inhibitory effects of these compounds on Aurora A kinase, but no obvious inhibition was observed for any compounds at 100 nM (Inhibition rate < 50%, **Figure S4**), demonstrating excellent selectivity for Aurora B.

The molecular docking illustrated the interactions between **3-17k** and the active site of Aurora B. It can embed well into the binding pocket, with its phenylurea (hydrophobic moiety) inserted deep into the cavity while the diethylamino (hydrophilic groups) face the solvent-exposed region. This further validated the accuracy of our constructed pharmacophore model and virtual screening result. Compound **3-17k** formed hydrogen bonds with Leu99, Gln145, GLU171 and ALA173, where GLU171 and ALA173 in the hinge region which also interacted with the original ligand **BI-847325** (Fig. 7A and **B**).

Moreover, through EPS map (electrostatic potential surface map) (Fig. 7C), The residues around the phenylurea moiety of **3-17k**, predominantly exhibited positive charges (blue), while the inductive effect of the halogen renders the 3-position fluorine atom negatively charged. This complementary electrostatic interaction significantly enhances binding affinity, thereby endowing the **3-17k** with optimal inhibiton activity.

After that, four tumor cell lines (Hela, HGC-27, HT-29, MCF-7) were employed to assess compounds efficacy (Table 1). Consistent with our hypothesis, compounds **3-17a**, **3-17d** and **3-17k** exhibited the strongest inhibitory activity against HGC27 and HT-29 cells, but showed no significant effects on HELA and MCF-7cells, followed by **3-17c**, **3-17f**, **3-17h**, **3-17i**, **3-17j**, **3-17m**. Following the initial screening, the selectivity profiles of three compounds (**3-17a**, **3-17d** and **3-17k**) were assessed in two normal cell types (GES-1, NCM460). The data demonstrated that

3-17k displayed a more favorable selectivity (SI = 98.29 for GES-1; SI = 77.47 for NCM460) than Hesperadin, which currently in clinical trials.

We also evaluated the inhibitory effects of the **3-17k** on four Aurora B over-expressing cell lines, including OVCAR8,

T24, NCIH1299 and SW480. As shown in Fig. 8, the compound exhibited micromolar-range IC_{50} values against all four cell lines, with the strongest effects observed in OVCAR8 and SW480 cells, suggested potential therapeutic efficacy against colorectal cancer. A discrepancy existed between the inhibitory effects of **3-17k** on cells versus kinase enzymes. This mainly resulted from its intrinsic properties, particularly membrane permeability and plasma protein binding. In any case, compound **3-17k** merited additional structural optimization and in-depth pharmacological studies.

2.4 Molecular dynamics simulation

The docked complexes of **3-17k** with Aurora B (PDB code: 5EYK) in docking experiments was considered as the initial structures for the MD run. The software Gromacs was used to model molecular dynamics for 100 ns.

Root mean square deviation (RMSD)

Root-mean-square deviation (RMSD) analysis revealed stable conformational dynamics of the protein-ligand system (Fig. 9). The **3-17k**_5EYK complex exhibited RMSD fluctuations within the acceptable range of 1.4–3.5 Å, reaching equilibrium at 55 ns and maintaining stability below 3.0 Å throughout the remaining simulation. Notably, the protein backbone demonstrated particularly low fluctuations, indicating structural preservation relative to the initial conformation. While the ligand (**3-17k**) displayed moderate positional deviations (40–90 ns) during the binding adaptation phase, it subsequently achieved stable binding mode persistence. These observations collectively suggest: maintenance of overall protein structural integrity, and establishment of stable ligand-protein interactions following initial binding-site accommodation.

Root mean square fluctuation (RMSF)

The root-mean-square fluctuation (RMSF) analysis of Aurora B kinase (5EYK) in complex with **3-17k** is presented in Fig. 10. The protein exhibited residue-specific fluctuations ranging from 0.52 to 7.00 Å throughout the simulation. Notably, four loop regions demonstrated particularly high flexibility: Ala81-Lys85, Asp162-Arg165, Pro242-Leu253, and Leu351-Gln356. In contrast, the binding site region (Pro98-Phe104) showed significantly reduced fluctuations, suggesting structural stabilization through specific interactions between **3-17k** and the

kinase. This observed rigidity in the binding pocket likely reflects the formation of stable molecular contacts that maintain the protein's active conformation.

Radius of gyration (Rg)

The radius of gyration (Rg) serves as an important indicator of protein compactness, with lower values corresponding to more folded structural conformations. As shown in Fig. 11, the **3-17k**_5EYK complex underwent significant conformational changes at approximately 20 ns during the simulation. Following this transition, the Rg values stabilized, maintaining an average of 21.10 Å throughout the remaining simulation time, suggesting achievement of a stable folded state.

Hydrogen bonds analysis

Hydrogen bonding represents a crucial stabilizing interaction in protein-ligand complexes. To characterize these interactions between **3-17k** and Aurora B kinase (5EYK), we analyzed hydrogen bond formation throughout the 100 ns molecular dynamics simulation (Fig. 12). The system demonstrated

dynamic hydrogen bonding patterns, with bond formation stabilizing after 2.43 ns and reaching a maximum of six simultaneous hydrogen bonds. Notably, these interactions remained stable throughout the simulation trajectory, indicating strong binding affinity and conformational stability of the **3-17k**_5EYK complex.

Binding free energy calculation (ΔG_{bind})

The binding affinity between compound **3-17k** and Aurora B kinase (PDB: 5EYK) was evaluated by calculating the total binding free energy (ΔG_{bind}) using the MM/PBSA method. This analysis incorporated van der Waals interactions, electrostatic contributions, and polar/nonpolar solvation energies. The results demonstrated strong binding affinity, with the **3-17k_5EYK** complex exhibiting a remarkably low ΔG_{bind} of -33.34 kcal·mol. Notably, van der Waals interactions (-53.34 kcal·mol) constituted the dominant contribution to the ΔG_{bind}.

The folding free-energy landscape (FEL) was constructed to characterize the conformational dynamics of the protein-ligand complex during molecular dynamics simulations. Using principal components PC1 and PC2 as reaction coordinates (Fig. 13), the FEL revealed a single, well-defined minimum free-energy basin that emerged at 99 ns. Structural analysis of this lowest-energy conformation showed that **3-17k** forms four stable hydrogen bonds with key residues Gly100, Glu171, Ala173, and Ala233, consistent with the hydrogen bond analysis presented in Fig. 11.

3. Conclusion

A potent and selective indolinone-based Aurora B inhibitor **3-17k** was successfully identified using FBDD and virtual screening. We adapted the modular assembly approach to synthesize target compounds and performed a SAR exploration for the Aurora B inhibition and four types of tumor cells. Compound **3-17a**, **3-17d** and **3-17k** had IC_{50} in the nanomolar range (1.100, 1.518 and 0.8911 nM, respectively) against Aurora B and showed a potent inhibitory activity against HGC27, HT-29, OVCAR8, T24, NCIH1299 and SW480 cells in the micromolar range as well. The most active **3-17k** was subjected to molecular dynamics (MD) simulations and exhibited a favorable binding free energy of -33.34 kcal·mol. The strategic implementation of a design approach centered around indolinone holds considerable potential for the discovery of novel and selective Aurora B inhibitors.

4. Experimental

4.1 Design and virtual screening

FBDD

In PyCharm, we utilized the *Recap* module from RDKit to perform fragmentation on reported Aurora B kinase inhibitors. These fragments were then recombined using the BRICS algorithm, generating a total

of 3,577 novel small molecules. The Python scripts for *Recap* and *BRICS* are available in the GitHub *(*https://github.com).

Pharmacophore generation

The pharmacophore model based on the receptor-ligand co-crystal structure (SBP) was generated using the *Catalyst* SBP module in *Discovery Studio* (DS). The derived pharmacophores was validated with active and inactive compounds separately. We performed preliminary screening of the enumerated library using Pharmacophore_07 and Pharmacophore_09. All ligands in the library were mapped to the pharmacophores, and their Fit values were calculated. During the screening, a flexible fitting strategy was employed to ensure optimal mapping, allowing ligands and pharmacophores to match in different conformations. Finally, compounds with Fit values below 2.5 were excluded, resulting in the initial identification of 410 high-scoring

compounds from the library of 3,577 molecules. The detailed procedures was described in SI.

Molecular Docking

The Aurora B (PDB code: 5EYK) was downloaded from the Protein Data Bank (http://www.rcsb.org). The protein preparation wizard in AutoDock vina was used to prepare them by taking off the water molecules and adding hydrogen atoms. Compounds docked with 5EYK following energy minimization (OPLS4 force field). The binding site was determined to be a sphere with a radius of 10 Å surrounding the template molecule prior to docking. Every parameter was left at its default setting for the simulated annealing. The docking process yielded 10 of the best ligand-receptor conformations, the results were visualized and analyzed using UCSF *Chimera* 1.19 with emphasis on key residue interactions and binding pose clustering. After HTVS and precise docking, top 20 compounds were identified. Finally, the architecture **3** was recognized as privileged scaffold via screening of synthetic accessibility and “Lipinski's rule of five".

Molecular dynamics simulation (MD)

A 100 ns Molecular dynamics (MD) simulation was conducted with *Gromacs* 2022.3 and the detailed procedures was described in SI [20].

4.2 Chemistry

The general procedures for the synthesis of compounds **3–3**

Under an inert atmosphere at 0°C, substituted phenyl isocyanate **3 – 2** (1 mmol) was added to a solution of **3 – 1** (1 mmol 6-amino-2-indolinone) in anhydrous DCM (5 mL). The reaction mixture was then warmed to room temperature and stirred for 24 h. After completion monitored by TLC, the DCM was removed under reduced pressure. The residue was washed with water (20 mL) and extracted with ethyl acetate (3 × 20 mL). Subsequent purification steps including aqueous washing, drying over anhydrous Na_2SO_4, filtration, solvent evaporation, and silica gel column chromatography afforded compound **3–3**.

1-(3-chlorophenyl)-3-(2-oxoindolin-6-yl)urea (3-3a). Grey solid, yield 79%, mp 179.3.7-181.4°C. ^{1}H NMR (500 MHz, DMSO- d_6) δ 10.34 (s, 1H), 8.83 (s, 1H), 8.76 (s, 1H), 7.69 (s, 1H), 7.34–7.18 (m, 4H), 7.08 (d, J = 7.9 Hz, 1H), 7.01 (d, J = 7.7 Hz, 1H), 6.81 (d, J = 8.0 Hz, 1H), 3.39 (s, 2H). ^{13}C NMR (125 MHz, DMSO- d_6) δ 176.83, 152.32, 144.15, 141.27, 138.91, 133.19, 130.40, 124.46, 121.42, 119.00, 117.53, 116.62, 110.84, 100.15, 35.35. HRMS (ESI) *m/z*: calcd for $C_{15}H_{12}ClN_3O_2$ $[M + H]^+$ 302.0691, found 302.0691.

1-(2-oxoindolin-6-yl)-3-(3-(trifluoromethyl) phe nyl)urea (3-3b). Grey solid, yield 89%, mp 188.7-191.4°C. ^{1}H NMR (500 MHz, DMSO- d_6) δ 10.33 (s, 1H), 9.01 (s, 1H), 8.82 (s, 1H), 8.01 (s, 1H), 7.58–7.47 (m, 2H), 7.30 (d, J = 8.0 Hz, 1H), 7.26 (s, 1H), 7.09 (d, J = 8.0 Hz, 1H), 6.83 (d, J = 2.0 Hz, 1H), 3.39 (s, 2H). ^{13}C NMR (125 MHz, DMSO- d_6) δ 176.82, 152.45, 144.15, 140.59, 138.86, 129.91, 125.31, 124.45, 123.15, 121.79, 119.06, 118.05, 114.07, 110.91, 100.22, 35.36. HRMS (ESI) *m/z*: calcd for $C_{16}H_{12}F_3N_3O_2$ $[M + H]^+$ 336.0954, found 336.0951.

1-(3-cyanophenyl)-3-(2-oxoindolin-6-yl)urea (3-3c). Grey solid, yield 86%, mp 148.2-153.7°C. ^{1}H NMR (500 MHz, DMSO- d_6) δ 10.35 (s, 1H), 9.03 (s, 1H), 8.90 (s, 1H), 7.96 (s, 1H), 7.66 (d, J = 8.2 Hz, 1H), 7.48 (t, J = 8.0 Hz, 1H), 7.41 (d, J = 7.8 Hz, 1H), 7.23 (s, 1H), 7.09 (d, J = 8.1 Hz, 1H), 6.83 (d, J = 8.0 Hz, 1H), 3.39 (s, 2H). ^{13}C NMR (125 MHz, DMSO- d_6) δ 176.84, 152.37, 144.16, 140.66, 138.81, 130.19, 125.28, 124.48, 122.85, 120.70, 119.14, 118.90, 111.60, 110.92, 100.19, 35.36. HRMS (ESI) *m/z*: calcd for $C_{16}H_{12}N_4O_2$ $[M + H]^+$ 293.1033, found 293.1024.

1-(2-oxoindolin-6-yl)-3-(m-tolyl)urea (3-3d). Grey solid, yield 85%, mp 144.3-147.9°C. ^{1}H NMR (500 MHz, DMSO- d_6) δ 10.56 (s, 1H), 8.97 (s, 1H), 8.84 (s, 1H), 7.53–7.42 (m, 3H), 7.37 (t, J = 7.8 Hz, 1H), 7.30 (d, J = 8.1 Hz, 1H), 7.06–6.97 (m, 2H), 3.50 (s, 2H), 2.73 (s, 3H). ^{13}C NMR (125 MHz, DMSO- d_6) δ 176.87, 152.48, 144.13, 139.64, 139.30, 137.95, 128.63, 124.60, 124.43, 122.54, 118.66, 115.31, 110.57, 99.93, 35.36, 21.25. HRMS (ESI) *m/z*: calcd for $C_{16}H_{15}N_3O_2$ $[M + H]^+$ 282.1237, found 282.1230.

1-(3-methoxyphenyl)-3-(2-oxoindolin-6-yl)urea (3-3e). Grey solid, yield 89%, mp 191.4-193.8°C. ^{1}H NMR (400 MHz, DMSO- d_6) δ 10.31 (s, 1H), 8.68 (s, 1H), 8.65 (s, 1H), 7.27 (s, 1H), 7.22–7.12 (m, 2H), 7.07 (d, J = 8.0 Hz, 1H), 6.90 (d, J = 7.8 Hz, 1H), 6.78 (d, J = 8.0 Hz, 1H), 6.54 (d, J = 8.3 Hz, 1H), 3.73 (s, 3H), 3.39 (s, 2H). ^{13}C NMR (100 MHz, $CDCl_3$) δ 176.83, 159.69, 152.32, 144.13, 143.99, 140.92, 139.16, 129.54, 124.44, 118.69, 110.62, 107.25, 103.85, 99.95, 54.91, 35.34. HRMS (ESI) *m/z*: calcd for $C_{16}H_{15}N_3O_3$ $[M + H]^+$ 298.1186, found 298.1181.

1-(3-nitrophenyl)-3-(2-oxoindolin-6-yl)urea (3-3f). Grey solid, yield 59%, mp 195.71–198.4°C. ^{1}H NMR (500 MHz, DMSO- d_6) δ 10.34 (s, 1H), 9.20 (s, 1H), 8.88 (s, 1H), 8.55 (d, 1H), 7.81 (d, J = 8.1 Hz, 1H), 7.69 (d, J = 7.9 Hz, 1H), 7.55 (t, J = 8.1 Hz, 1H), 7.26 (s, 1H), 7.09 (d, J = 8.0 Hz, 1H), 6.85 (d, J = 8.0 Hz, 1H), 3.40 (s, 2H). ^{13}C NMR (125 MHz, DMSO- d_6) δ 176.84, 152.39, 148.16, 144.17, 141.07, 138.75, 130.05, 124.47,

124.28, 119.22, 116.25, 112.10, 111.03, 100.32, 35.38. HRMS (ESI) *m/z*: calcd for $C_{15}H_{12}N_4O_4$ $[M-H]^-$ 311.0786, found 311.0784.

1-(3-fluorophenyl)-3-(2-oxoindolin-6-yl)urea (3-3g). Grey solid, yield 81%, mp 167.3-169.7°C. ^{1}H NMR (500 MHz, DMSO- d_6) δ 10.34 (s, 1H), 8.91 (s, 1H), 8.80 (s, 1H), 7.48 (d, J = 11.9 Hz, 1H), 7.33–7.23 (m, 2H), 7.13–7.05 (m, 2H), 6.84–6.73 (m, 2H), 3.39 (s, 2H). ^{13}C NMR (100 MHz, DMSO- d_6) δ 176.81, 163.60, 161.20, 152.31, 144.14, 141.53, 138.93, 130.26, 124.46, 118.96, 113.90, 110.79, 107.99, 104.93, 100.10, 35.34. HRMS (ESI) *m/z*: calcd for $C_{15}H_{12}FN_3O_2$ $[M + H]^+$ 286.0986, found 286.0982.

The general procedures for the synthesis of compounds **3–6**

Compound **3–4** (1 mmol), EDC·HCl (1.2 mmol), and HOBt (1.2 mmol) were sequentially dissolved in DMF (3 mL) and stirred under a nitrogen atmosphere at 0–4°C for 20 minutes. Subsequently, compound **3–5** (1.2 mmol) was added to the mixture, followed by stirring at 0–4°C for 30 minutes. The reaction was then allowed to warm to room temperature and stirred for an additional 24 hours. After reaction completion confirmed by TLC, the residue was washed with water (30 mL) and extracted with ethyl acetate (6 × 30 mL). The combined organic phases were further washed with copious amounts of water (3 × 50 mL), then dried over anhydrous sodium sulfate, filtered, concentrated under reduced pressure, and purified by silica gel column chromatography to afford compound **3–6**.

5-formyl-2,4-dimethyl-N-(2-(pyrrolidin-1-yl)ethyl)-1H-pyrrole-3-carboxamide (3-6a). Yellow solid, yield 91%, mp 144.2-147.9°C. ^{1}H NMR (500 MHz, $CDCl_3$) δ 9.56 (s, 1H), 6.36 (s, 1H), 3.52 (q, J = 5.5 Hz, 2H), 2.72 (t, J = 5.9 Hz, 2H), 2.61–2.54 (m, 4H), 2.48 (s, 3H), 2.45 (s, 3H), 1.82–1.72 (m, 4H). ^{13}C NMR (100 MHz, $CDCl_3$) δ 177.21, 165.16, 139.65, 131.42, 128.21, 119.25, 54.60, 53.86, 37.99, 23.66, 13.56, 10.17. HRMS (ESI) *m/z*: calcd for $C_{14}H_{21}N_3O_2$ $[M + H]^+$ 264.1707, found 264.1700.

N-(2-(diethylamino)ethyl)-5-formyl-2,4-dimethyl-1H-pyrrole-3-carboxamide (3-6b). Yellow solid, yield 93%, mp 135.1-138.4°C. ^{1}H NMR (500 MHz, $CDCl_3$) δ 10.31 (s, 1H), 9.55 (s, 1H), 6.44 (s, 1H), 3.48–3.42 (m, 2H), 2.62 (t, J = 5.9 Hz, 2H), 2.58–2.47 (m, 10H), 1.00 (t, J = 7.1 Hz, 6H). ^{13}C NMR (125 MHz, $CDCl_3$) δ 177.16, 165.15, 140.28, 132.16, 128.16, 119.05, 51.36, 46.44, 36.79, 13.71, 11.92, 10.43. HRMS (ESI) *m/z*: calcd for $C_{14}H_{23}N_3O_2$ $[M + H]^+$ 266.1863, found 266.1838.

The procedures for the synthesis of compounds **3–9**

Compound **3–7** (1 mmol), **3–8** (2 mmol), and K_2CO_3 (3 mmol) were dissolved in 5 mL of acetonitrile, stirred and refluxed the mixture at 60°C for 8 hours. After the reaction, dilute the mixture with 20 mL of water and extract with ethyl acetate (3 × 20 mL). Combine the organic phases, dry over anhydrous sodium sulfate, concentrate under reduced pressure, and purify by silica gel column chromatography to obtain the target compound **3–9**.

3-bromo-1H-pyrazol-5-amine (3–9). Light yellow solid, yield 50%, mp 165.8-168.7°C. ^{1}H NMR (500 MHz, $CDCl_3$) δ 7.83 (s, 1H), 5.98 (s, 1H), 2.44 (q, J = 7.5 Hz, 2H), 1.26 (t, J = 7.6 Hz, 3H). ^{13}C NMR (100 MHz, DMSO- d_6) δ 171.53, 139.73, 124.86, 95.36, 28.57, 9.36. HRMS (ESI) *m/z*: calcd for $C_6H_8BrN_3O$ $[M + H]^+$ 217.9924, found 217.9920.

The procedures for the synthesis of compounds **3–11**

Compound **3–9** (1 mmol), 3–10 (1.2 mmol), K_2CO_3 (3 mmol), $Pd(PPh_3)_4$, **(**0.05 mmol**)** were fixed into a 15 mL sealed tube. Then 5 mL 1,4-dioxane was added, followed by the addition of 1 mL of H_2O. Purge the reaction mixture with argon (Ar) gas for 20 minutes, and then heat the reaction at 105°C for 18 hours. After completion of the reaction (monitored by TLC or LCMS), dilute the mixture with 20 mL of water and extract with ethyl acetate (5 × 20 mL). Combine the organic layers, dry over anhydrous sodium sulfate, concentrate under reduced pressure, and purify by silica gel column chromatography to afford the target compound **3–11**.

N-(3-(2-oxoindolin-6-yl)-1*H*-pyrazol-5-yl)propionamide **(3–11).** Powdery white solid, yield 56%, mp 246.5-251.7°C. ^{1}H NMR (500 MHz, DMSO- d_6) δ 12.75 (s, 1H), 10.52 (s, 1H), 10.35 (s, 1H), 7.30–7.19 (m, 2H), 7.10 (s, 1H), 6.80 (s, 1H), 3.49 (s, 2H), 2.30 (q, J = 7.6 Hz, 2H), 1.06 (t, J = 7.6 Hz, 3H). ^{13}C NMR (100 MHz, DMSO- d_6) δ 171.53, 139.73, 124.86, 95.36, 28.57, 9.36. HRMS (ESI) *m/z*: calcd for $C_{14}H_{14}N_4O_2$ $[M + H]^+$ 271.1190, found 271.1189.

The procedures for the synthesis of compounds **3–14**

The compound **3–12** (1 mmol), **3–13** (1.2 mmol) and K_2CO_3 (1.2 mmol) were dissolved in 5 mL acetonitrile and stirred under reflux at 80°C for 4 hours. After completion of the reaction (confirmed by TLC or LCMS), dilute the mixture with 15 mL of water and extract with ethyl acetate (3 × 15 mL). Combine the organic layers, dry over anhydrous sodium sulfate (Na_2SO_4), concentrate under reduced pressure, and purify by silica gel column chromatography to afford the target compound **3–14**.

1-(2-((tert-butyldimethylsilyl)oxy)ethyl)-1H-pyrazole-4-carbal dehyde (3–14). Yellow oil, yield 71%. ^{1}H NMR (500 MHz, DMSO- d_6) δ 9.79 (s, 1H), 8.40 (s, 1H), 7.99 (s, 1H), 4.26 (t, J = 5.2 Hz, 2H), 3.92 (t, J = 5.2 Hz, 2H), 0.77 (s, 9H), -0.10 (s, 6H). ^{13}C NMR (125 MHz, DMSO- d_6) δ 184.52, 139.93, 135.49, 123.63, 61.25, 54.22, 25.58, 17.78, 5.73. HRMS (ESI) *m/z*: calcd for $C_{12}H_{22}N_2O_2Si$ $[M + H]^+$ 255.1523, found 255.1521.

The procedures for the synthesis of compounds **3–16**

The compound **3** – **1** (1 mmol), **3–15 (**1.2 mmol), K_2CO_3 (2 mmol), a catalytic amount of KI were dissolved in a round-bottom flask. The 5mL THF was added and the mixture was stirred t at room temperature for 16 hours. Upon reaction completion (monitored by TLC or LCMS), 25 mL water was added and extract with ethyl acetate (5 × 25 mL). The Combined the organic phases was dried over with

Na_2SO_4, concentrated under reduced pressure, and purify by silica gel column chromatography to obtain the target compound **3–16**.

The general procedures for the synthesis of compounds **3-17a**-**3-17k**

Compound **3–3** (1.2 mmol) was dissolved in 5 mL of methanol, followed by the addition of 1 mL of 50% aqueous KOH solution. The mixture was stirred at room temperature for 15 minutes and **3–6** (1 mmol) was added. The reaction mixture was then stirred overnight at room temperature. Upon completion of the reaction as monitored by TLC, methanol was removed under reduced pressure. The residue was diluted with 10 mL of hot water, and the pH was adjusted to 7.0 with dilute hydrochloric acid. A solid precipitate was formed, which was collected by filtration and washed. The purification of the target compounds was achieved by recrystallization from methanol.

If the target compounds could not be obtained through methanol recrystallization, an alternative purification procedure was employed. The mixture was extracted with 25 mL of water and ethyl acetate (5 × 25 mL). The organic layers were combined, dried over anhydrous sodium sulfate, and concentrated under reduced pressure. Final purification was performed by silica gel column chromatography to obtain the target compounds **3-17a-3-17k**.

(Z)-5-((6-(3-(3-chlorophenyl)ureido)-2-oxoindolin-3-ylidene)methyl)-2,4-dimethyl-N-(2-(pyrrolidin-1-yl)ethyl)-1H-pyrrole-3-carboxamide (3-17a). Orange solid, yield 65%, mp 291.1-296.4°C. ^{1}H NMR (500 MHz, DMSO- d_6) δ 13.46 (s, 1H), 10.86 (s, 1H), 8.89 (s, 2H), 7.71 (s, 1H), 7.66 (d, J = 8.2 Hz, 1H), 7.50–7.44 (m, 2H), 7.33–7.24 (m, 3H), 7.02 (d, J = 7.4 Hz, 1H), 6.92 (d, J = 8.7 Hz, 1H), 2.56 (t, J = 6.9 Hz, 2H), 2.49–2.46 (m, 4H), 2.42 (s, 3H), 2.37 (s, 3H), 1.71–1.64 (m, 4H). ^{13}C NMR (125 MHz, DMSO- d_6) δ 169.95, 164.76, 152.26, 141.29, 139.11, 138.39, 134.87, 133.20, 130.42, 128.00, 125.74, 121.59, 121.45, 120.29, 119.58, 119.14, 117.56, 116.67, 115.54, 111.24, 100.15, 54.83, 53.53, 38.04, 23.21, 13.19, 10.47. HRMS (ESI) *m/z*: calcd for $C_{29}H_{31}ClN_6O_3$ $[M + H]^+$ 547.2219, found 547.2208.

(Z)-2,4-dimethyl-5-((2-oxo-6-(3-(3-(trifluoromethyl)phenyl)ureido)indolin-3-ylidene)methyl)-N-(2-(pyrrolidin-1-yl)ethyl)-1H-pyrrole-3-carboxamide (3-17b). Orange solid, yield 71%, mp 267.1-273.5°C. ^{1}H NMR (500 MHz, DMSO- d_6) δ 13.47 (s, 1H), 10.85 (s, 1H), 9.06 (s, 1H), 8.93 (s, 1H), 8.03 (s, 1H), 7.66 (d, J = 8.4 Hz, 1H), 7.61–7.42 (m, 4H), 7.33–7.28 (m, 2H), 6.94 (d, J = 8.4 Hz, 1H), 2.42 (s, 3H), 2.38 (s, 3H), 1.73–1.65 (s, 4H). ^{13}C NMR (125 MHz, DMSO- d_6) δ 169.93, 164.73, 152.38, 140.60, 139.10, 138.31, 134.87, 129.92, 129.40, 128.02, 125.73, 125.32, 123.16, 121.84, 121.62, 120.30, 119.64, 119.12, 118.04, 115.52, 114.11, 111.30, 100.23, 79.18, 54.83, 53.52, 38.03, 23.21, 13.18, 10.46. HRMS (ESI) *m/z*: calcd for $C_{30}H_{31}F_3N_6O_3$ $[M + H]^+$ 581.2482, found 581.2473.

(Z)-5-((6-(3-(3-cyanophenyl)ureido)-2-oxoindolin-3-ylidene)methyl)-2,4-dimethyl-N-(2-(pyrrolidin-1-yl)ethyl)-1H-pyrrole-3-carboxamide (3-17c). Orange solid, yield 74%, mp 277.3-281.2°C. ^{1}H NMR (400 MHz, DMSO- d_6) δ 13.41 (s, 1H), 10.80 (s, 1H), 8.98 (s, 1H), 8.92 (s, 1H), 7.92 (s, 1H), 7.61 (t, J = 7.6 Hz, 2H), 7.51–7.32 (m, 4H), 7.24 (s, 1H), 6.87 (d, J = 8.4 Hz, 1H), 3.30–3.22 (m, 2H)(overlap), 2.46–2.39 (m,

6H) (overlap), 2.31 (s, 6H), 1.62 (q, *J* = 3.3 Hz, 4H). ^{13}C NMR (100 MHz, DMSO- d_6) δ 169.92, 164.72, 152.27, 140.64, 139.09, 138.23, 134.87, 130.17, 128.01, 125.72, 125.28, 122.88, 121.61, 120.75, 120.28, 119.69, 119.11, 118.88, 115.49, 111.59, 111.28, 100.20, 54.80, 53.51, 38.00, 23.19, 13.17, 10.45. HRMS (ESI) *m/z*: calcd for $C_{30}H_{31}N_7O_3$ $[M + H]^+$ 538.2561, found 538.2549.

(Z)-2,4-dimethyl-5-((2-oxo-6-(3-(m-tolyl)ureido)indolin-3-ylidene)methyl)-N-(2-(pyrrolidin-1-yl)ethyl)-1H-pyrrole-3-carboxamide (3-17d). Orange solid, yield 75%, mp 269.5-273.9°C. ^{1}H NMR (400 MHz, DMSO- d_6) δ 13.40 (s, 1H), 10.79 (s, 1H), 8.80 (s, 1H), 8.60 (s, 1H), 7.58 (d, *J* = 8.3 Hz, 1H), 7.41 (s, 2H), 7.26 (d, *J* = 7.6 Hz, 2H), 7.21–7.05 (m, 2H), 6.84 (d, *J* = 8.4 Hz, 1H), 6.74 (s, 1H), 2.46–2.39 (m, 9H), 2.36 (s, 3H), 2.32 (s, 3H), 2.22 (s, 4H), 1.66–1.59 (m, 4H). ^{13}C NMR (100 MHz, DMSO- d_6) δ 169.96, 164.74, 152.39, 139.63, 139.13, 138.80, 137.92, 134.72, 128.61, 127.82, 125.71, 122.54, 121.35, 120.23, 119.22, 119.11, 118.71, 115.65, 115.37, 110.97, 99.91, 54.81, 53.51, 38.02, 23.20, 21.23, 13.16, 10.44. HRMS (ESI) *m/z*: calcd for $C_{30}H_{34}N_6O_3$ $[M + H]^+$ 527.2765, found 527.2754.

(Z)-5-((6-(3-(3-chlorophenyl)ureido)-2-oxoindolin-3-ylidene)methyl)-N-(2-(diethylamino)ethyl)-2,4-dimethyl-1H-pyrrole-3-carboxamide (3-17e). Orange solid, yield 61%, mp 296.1-300.4°C. ^{1}H NMR (500 MHz, DMSO- d_6) δ 13.48 (s, 1H), 10.86 (s, 1H), 8.94 (s, 1H), 7.78–7.60 (m, 3H), 7.48 (s, 1H), 7.40–7.23 (m, 5H), 7.04–6.98 (m, 1H), 6.92 (d, *J* = 8.3 Hz, 1H), 3.28 (q, *J* = 6.2 Hz, 2H), 2.43 (s, 3H), 2.39 (s, 3H), 0.97 (t, *J* = 7.1 Hz, 6H). ^{13}C NMR (125 MHz, DMSO- d_6) δ 169.95, 164.72, 152.27, 141.31, 139.12, 138.43, 134.95, 133.20, 130.40, 127.91, 125.73, 121.56, 120.10, 119.56, 119.13, 117.55, 116.65, 115.60, 111.22, 100.14, 51.67, 46.52, 36.96, 13.30, 11.90, 10.59. HRMS (ESI) *m/z*: calcd for $C_{29}H_{33}ClN_6O_3$ $[M + H]^+$ 549.2375, found 549.2366.

(Z)-N-(2-(diethylamino)ethyl)-2,4-dimethyl-5-((2-oxo-6-(3-(3-(trifluoromethyl)phenyl)ureido)indolin-3-ylidene)methyl)-1H-pyrrole-3-carboxamide (3-17f). Orange solid, yield 67%, mp 281.5–286.0°C. ^{1}H NMR (500 MHz, DMSO- d_6) δ 13.48 (s, 1H), 10.86 (s, 1H), 9.04 (s, 1H), 8.91 (s, 1H), 8.03 (s, 1H), 7.66 (d, *J* = 8.3 Hz, 1H), 7.57 (d, *J* = 8.3 Hz, 1H), 7.54–7.47 (m, 2H), 7.37 (t, *J* = 5.6 Hz, 1H), 7.33–7.28 (m, 2H), 6.94 (d, *J* = 8.3 Hz, 1H), 3.28 (q, *J* = 6.5 Hz, 2H), 2.43 (s, 3H), 2.39 (s, 3H), 0.97 (t, *J* = 7.1 Hz, 6H). ^{13}C NMR (125 MHz, DMSO- d_6) δ 169.93, 164.71, 152.37, 140.58, 139.11, 138.31, 134.98, 129.92, 129.65, 127.96, 127.47, 125.73, 121.85, 121.62, 120.12, 119.65, 119.13, 118.05, 115.57, 114.11, 111.30, 100.23, 51.68, 46.52, 36.96, 13.30, 11.89, 10.59. HRMS (ESI) *m/z*: calcd for $C_{30}H_{33}F_3N_6O_3$ $[M + H]^+$ 583.2639, found 583.2629.

(Z)-5-((6-(3-(3-cyanophenyl)ureido)-2-oxoindolin-3-ylidene)methyl)-N-(2-(diethylamino)ethyl)-2,4-dimethyl-1H-pyrrole-3-carboxamide (3-17g). Orange solid, yield 65%, mp 271.6-276.1°C. ^{1}H NMR (500 MHz, DMSO- d_6) δ 13.48 (s, 1H), 10.87 (s, 1H), 9.19–8.99 (m, 2H), 7.98 (s, 1H), 7.71–7.61 (m, 2H), 7.55–7.28 (m, 5H), 6.97–6.90 (m, 1H), 3.33–3.25 (m, 4H), 2.61–2.52 (m, 4H, overlap), 2.43 (s, 3H), 2.39 (s, 3H), 0.99 (t, *J* = 7.1 Hz, 6H). ^{13}C NMR (125 MHz, DMSO- d_6) δ 169.95, 164.78, 152.32, 140.69, 139.12, 138.31, 135.02, 130.20, 127.97, 125.74, 125.29, 122.90, 121.63, 120.75, 120.07, 119.68, 119.16, 118.91, 115.59, 111.60,

111.31, 100.21, 51.61, 46.54, 36.84, 13.32, 11.76, 10.60. HRMS (ESI) *m/z*: calcd for $C_{30}H_{33}N_7O_3$ $[M + H]^+$ 540.2718, found 540.2706.

(Z)-N-(2-(diethylamino)ethyl)-2,4-dimethyl-5-((2-oxo-6-(3-(m-tolyl)ureido)indolin-3-ylidene)methyl)-1H-pyrrole-3-carboxamide (3-17h). Orange solid, yield 69%, mp 264.2-259.3°C. ^{1}H NMR (500 MHz, DMSO- d_6) δ 13.47 (s, 1H), 10.85 (s, 1H), 8.80 (s, 1H), 8.61 (s, 1H), 7.64 (d, J = 8.3 Hz, 1H), 7.47 (s, 1H), 7.37 (t, J = 5.5 Hz, 1H), 7.31 (d, J = 8.3 Hz, 1H), 7.23 (d, J = 8.1 Hz, 1H), 7.15 (t, J = 7.8 Hz, 1H), 6.90 (d, J = 8.4 Hz, 1H), 6.79 (d, J = 7.5 Hz, 1H), 3.28 (q, J = 6.5 Hz, 2H), 2.58–2.51 (m, 4H, overlap), 2.43 (s, 3H), 2.39 (s, 3H), 2.28 (s, 3H), 0.98 (t, J = 7.1 Hz, 6H). ^{13}C NMR (125 MHz, DMSO- d_6) δ 169.97, 164.75, 152.40, 139.61, 139.15, 138.80, 137.96, 134.88, 128.64, 127.80, 125.73, 122.59, 121.39, 120.06, 119.26, 119.15, 118.72, 115.70, 115.39, 111.00, 99.93, 51.66, 46.53, 36.94, 21.25, 13.30, 11.87, 10.59. HRMS (ESI) *m/z*: calcd for $C_{30}H_{36}N_6O_3$ $[M + H]^+$ 529.2922, found 529.2910.

(Z)-N-(2-(diethylamino)ethyl)-5-((6-(3-(3-methoxyphenyl)ureido)-2-oxoindolin-3-ylidene)methyl)-2,4-dimethyl-1H-pyrrole-3-carboxamide (3-17i). Orange solid, yield 71%, mp 292.0-296.4°C. ^{1}H NMR (500 MHz, DMSO- d_6) δ 13.47 (s, 1H), 10.86 (s, 1H), 8.94 (s, 1H), 8.82 (s, 1H), 7.65 (d, J = 8.3 Hz, 1H), 7.48 (s, 1H), 7.25–7.34 (m, 4H), 7.05–6.98 (m, 2H), 6.96–6.89 (m, 2H), 3.73 (s, 3H), 3.39–3.31 (m, 2H, overlap), 2.65–2.49 (m, 6H, overlap), 2.42 (s, 3H), 2.38 (s, 3H), 0.98 (t, J = 7.1 Hz, 6H). ^{13}C NMR (125 MHz, DMSO- d_6) δ 169.97, 164.75, 163.36, 161.32, 148.35, 141.59, 139.15, 138.42, 134.45, 130.28, 127.80, 125.73, 121.39, 120.06, 119.26, 119.15, 115.70, 113.92, 111.00, 104.69, 100.69, 54.93, 51.63, 46.54, 36.87, 13.30, 11.80, 10.60. HRMS (ESI) *m/z*: calcd for $C_{30}H_{36}N_6O_4$ $[M + H]^+$ 545.2871, found 545.2859.

(Z)-N-(2-(diethylamino)ethyl)-2,4-dimethyl-5-((6-(3-(3-nitrophenyl)ureido)-2-oxoindolin-3-ylidene)methyl)-1H-pyrrole-3-carboxamide (3-17j). Orange solid, yield 67%, mp 295.8-299.2°C. ^{1}H NMR (500 MHz, DMSO- d_6) δ 13.44 (s, 1H), 10.83 (s, 1H), 9.30 (s, 1H), 9.04 (s, 1H), 8.60–8.51 (m, 1H), 7.78 (d, J = 8.1 Hz, 1H), 7.68 (d, J = 8.2 Hz, 1H), 7.63 (d, J = 8.3 Hz, 1H), 7.53 (q, J = 8.3 Hz, 1H), 7.45 (s, 1H), 7.36–7.27 (m, 2H), 6.92 (d, J = 8.3 Hz, 1H), 3.28–3.20 (m, 2H), 2.53–2.42 (m, 6H), 2.35 (s, 6H), 0.93 (t, J = 7.1 Hz, 6H). ^{13}C NMR (125 MHz, DMSO- d_6) δ 169.97, 164.75, 163.39, 161.45, 148.27, 141.68, 139.15, 138.33, 134.88, 130.46, 128.64, 127.80, 125.73, 121.39, 120.06, 119.26, 119.15, 115.70, 113.89, 111.00, 104.87, 104.78, 100.09, 51.68, 46.52, 36.94, 13.29, 11.89, 10.88. HRMS (ESI) *m/z*: calcd for $C_{29}H_{33}N_7O_5$ $[M + H]^+$ 560.2616, found 560.2605.

(Z)-N-(2-(diethylamino)ethyl)-5-((6-(3-(3-fluorophenyl)ureido)-2-oxoindolin-3-ylidene)methyl)-2,4-dimethyl-1H-pyrrole-3-carboxamide (3-17k). Orange solid, yield 67%, mp 282.5-287.6°C. ^{1}H NMR (500 MHz, DMSO- d_6) δ 13.48 (s, 1H), 10.86 (s, 1H), 8.92 (s, 1H), 8.88 (s, 1H), 7.66 (d, J = 8.3 Hz, 1H), 7.53–7.47 (m, 2H), 7.39–7.26 (m, 3H), 7.12 (d, J = 8.2 Hz, 1H), 6.91 (d, J = 8.2 Hz, 1H), 6.78 (td, J = 8.5, 2.6 Hz, 1H), 3.28 (q, J = 6.5 Hz, 4H, overlap), 2.57–2.52 (m, 4H, overlap), 2.43 (s, 3H), 2.39 (s, 3H), 0.97 (t, J = 7.1 Hz, 6H). ^{13}C NMR (125 MHz, DMSO- d_6) δ 169.95, 164.72, 163.38, 161.46, 152.26, 141.65, 139.13, 138.42, 134.96, 130.37, 127.92, 125.74, 121.56, 120.12, 119.56, 119.15, 115.60, 113.95, 111.20, 108.21, 104.75, 100.12,

51.68, 46.52, 36.96, 13.29, 11.89, 10.88. HRMS (ESI) *m/z*: calcd for $C_{29}H_{33}FN_6O_3$ $[M + H]^+$ 533.2671, found 533.2657.

The general procedures for the synthesis of compounds **3-17l-3-17n**

A mixture of compound **3–11** or **3–16 (**1 mmol) and **3–6** or **3–14 (**1.2 mmol**)** were charged into a 50 mL round-bottom flask and dissolved in 5 mL of ethanol (EtOH). **A** catalytic amount of pyrrolidine was added, and the reaction mixture was stirred at 25–40°C for 8 hours. After completion of the reaction (monitored by TLC), the mixture was diluted with 20 mL of water and extracted with ethyl acetate (3 × 20 mL). The combined organic layers were dried over anhydrous sodium sulfate, concentrated under reduced pressure, and purified by silica gel column chromatography to afford the target compounds **3-17l-3-17n**.

(Z)-N-(2-(diethylamino)ethyl)-2,4-dimethyl-5-((2-oxo-6-(5-propionamido-1H-pyrazol-3-yl)indolin-3-ylidene)methyl)-1H-pyrrole-3-carboxamide (3-17l). Orange solid, yield 62%, mp 282.5-287.6°C. ^{1}H NMR (400 MHz, DMSO-d_6) δ 13.57 (s, 1H), 12.74 (s, 1H), 11.02 (s, 1H), 10.33 (s, 1H), 7.82 (d, J = 8.0 Hz, 1H), 7.63 (s, 1H), 7.46–7.28 (m, 2H), 7.16 (s, 1H), 6.81 (s, 1H), 3.30–3.22 (m, 2H, overlap), 2.46–2.55 (m, J = 7.0 Hz, 4H, overlap), 2.42 (s, 3H), 2.40 (s, 3H), 2.29 (q, J = 7.5 Hz, 2H), 1.05 (t, J = 7.6 Hz, 3H), 0.95 (t, J = 7.1 Hz, 6H).^{13}C NMR (125 MHz, DMSO- d_6) δ 169.93, 164.73, 152.24, 141.28, 139.09, 138.38, 134.83, 133.18, 130.39, 127.97, 125.71, 121.55, 120.27, 119.56, 119.11, 117.53, 116.13, 115.53, 111.20, 100.12, 54.80, 53.51, 38.00, 23.19, 13.17, 10.45. HRMS (ESI) *m/z*: calcd for $C_{29}H_{33}FN_6O_3$ $[M + H]^+$ 533.2671, found 533.2657.

(Z)-5-((6-((2-(cyclopropylamino)-2-oxoethyl)amino)-2-oxoindolin-3-ylidene)methyl)-N-(2-(diethylamino)ethyl)-2,4-dimethyl-1H-pyrrole-3-carboxamide (3-17m). Orange solid, yield 57%, mp 273.5-276.2°C. ^{1}H NMR (400 MHz, DMSO- d_6) δ 13.37 (s, 1H), 10.68 (s, 1H), 8.00 (s, 1H), 7.69–7.40 (m, 2H), 7.25 (s, 1H), 6.20 (d, J = 8.4 Hz, 1H), 6.11 (s, 2H), 3.60 (s, 2H), 3.41–3.38 (m, 2H), 2.91–2.69 (m, 6H), 2.70–2.59 (m, 1H), 2.42 (s, 3H), 2.36 (s, 3H), 1.09 (t, J = 7.3 Hz, 6H), 0.65–0.54 (m, 2H), 0.50–0.37 (m, 2H). ^{13}C NMR (100 MHz, DMSO- d_6) δ 171.11, 170.33, 165.27, 153.50, 148.40, 140.07, 133.82, 125.96, 125.73, 119.68, 119.03, 118.47, 117.09, 114.23, 109.55, 105.79, 94.05, 51.03, 46.80, 46.66, 22.27, 13.33, 10.60, 5.62. HRMS (ESI) *m/z*: calcd for $C_{27}H_{36}N_6O_3$ $[M + H]^+$ 493.2922, found 493.2920.

(Z)-N-(3-(3-((1-(2-hydroxyethyl)-1H-pyrazol-4-yl)methylene)-2-oxoindolin-6-yl)-1H-pyrazol-5-yl)propionamide (3-17n). Orange solid, yield 49%, mp 301.5-303.7°C. ^{1}H NMR (400 MHz, DMSO- d_6) δ 12.76 (s, 1H), 10.69 (s, 1H), 10.32 (s, 1H), 8.85 (s, 1H), 8.26 (s, 1H), 7.73 (s, 1H), 7.65 (d, J = 8.4 Hz, 1H), 7.33 (d, J = 8.0 Hz, 1H), 7.13 (s, 1H), 6.85 (s, 1H), 4.94 (s, 1H), 4.24 (t, J = 5.6 Hz, 2H), 3.77 (d, J = 6.4 Hz, 2H), 2.31 (q, J = 7.5 Hz, 2H), 1.07 (t, J = 7.5 Hz, 3H). ^{13}C NMR (100 MHz, DMSO- d_6) δ 171.23, 169.94, 167.31, 143.21, 140.91, 140.46, 135.29, 133.54, 131.44, 120.98, 119.31, 118.00, 117.84, 117.01, 115.68, 105.61, 57.76, 54.54, 29.70, 9.73. HRMS (ESI) *m/z*: calcd for $C_{20}H_{20}N_6O_3$ $[M + H]^+$ 393.1670, found 393.1668.

The procedures for the synthesis of compounds **3–19**

The compound 2-indolinone 3–18 (1.2 mmol) was dissolved in 5 mL of methanol, followed by addition of 1 mL of 50% aqueous KOH solution. The mixture was stirred at room temperature for 15 minutes, after which 1 mmol of *N*-(2-(diethylamino)ethyl)-5-formyl-2,4-dimethyl-1*H*-pyrrole-3-carboxamide 3-6b was added. The reaction mixture was stirred overnight at room temperature. Upon completion of the reaction, methanol was removed under reduced pressure. The residue was extracted with 20 mL of water and ethyl acetate (3 × 20 mL). The combined organic layers were dried over anhydrous sodium sulfate, concentrated under reduced pressure, and purified by silica gel column chromatography to afford the target compound **3–19**.

(Z)-N-(2-(diethylamino)ethyl)-2,4-dimethyl-5-((2-oxoindolin-3-ylidene)methyl)-1H-pyrrole-3-carboxamide (3–19). Orange solid, yield 74%, mp 233.1-236.9°C. ^{1}H NMR (500 MHz, $CDCl_3$) δ 13.26 (s, 1H), 9.00 (s, 1H), 7.43 (d, J = 7.5 Hz, 1H), 7.15 (t, J = 7.6 Hz, 1H), 7.05 (t, J = 7.5 Hz, 1H), 6.87 (d, J = 7.7 Hz, 1H), 6.73–6.68 (m, 1H), 3.54 (q, J = 5.4 Hz, 2H), 2.75–2.59 (m, 6H), 2.53 (s, 3H), 2.29 (s, 3H), 1.05 (t, J = 7.1 Hz, 6H). ^{13}C NMR (125 MHz, $CDCl_3$) δ 170.17, 166.04, 137.68, 137.43, 129.58, 126.46, 126.40, 126.29, 123.22, 121.87, 119.84, 117.79, 114.64, 109.61, 51.52, 46.20, 36.79, 14.15, 11.34, 11.10. HRMS (ESI) *m/z*: calcd for $C_{22}H_{28}N_4O_2$ $[M + H]^+$ 381.2285, found 381.2257

4.3 Biological activity

Kinase activity assay

The compound is diluted with DMSO (item number: D4540, manufacturer: Sigma) to 100× of different detection concentrations. 100 nL of the compound is transferred into a 384-well reaction plate (784075, Greiner) using the Echo 655 (ECHO®655 SYSTEM, Beckman). A 2× kinase solution is prepared with 1× kinase reaction buffer (1X Buffer, containing 5 mM $MgCl_2$, 1 mM DTT, H_2O, 1 mM $MnCl_2$, and 50 nM SEB). 5 μL of AURKB (6 nM, 08-113, Carna) solution is transferred into the 384-well reaction plate. The plate is centrifuged at 1000 rpm for 60 seconds, and then incubated at 25°C for 10 minutes. A 2× mixture of the substrate (TK: 1 μM) and ATP (25 μM) is prepared with the kinase reaction buffer. 5 μL of the substrate and ATP mixture is added to the reaction plate to initiate the reaction, and then the plate is centrifuged at 1000 rpm for 60 seconds. The plate is sealed with a plate sealer film and incubated at 25°C for 50 minutes. 10 μL of the kinase detection reagent is added to each well of the reaction plate, and then the plate is centrifuged at 1000 rpm for 1 minute, followed by incubation at 25°C for 60 minutes. The fluorescence signals at 620 nm (Cryptate) and 665 nm (XL665) are read using a BMG microplate reader.

Data analysis was performed using GraphPad 8.0 software. The following non - linear fitting formula was used to obtain the IC50 (half - maximal inhibitory concentration) of the compound:

Y = Bottom+(Top - Bottom)/(1 + 10^((LogIC50 - X)*Hill Slope))

X: Logarithm of the compound concentration,

Y: Percent inhibition.

Cell Toxicity Assay

During the logarithmic phase of cell growth, the medium was aspirated, washed with PBS, digested with trypsin, terminated with the addition of medium, gently blown and counted. Each cell line was seeded in 96-well plates (100 μL/well) at a density of 5×10^3 cells/ well, respectively, and cultured overnight. Compounds (20 μL/ well) were added, and a concentration gradient (0, 1, 10, 20, 30, and 40 μM) was set for each compound, with six replicate wells for each concentration. The cells were incubated in an incubator at 37°C for 48 h. MTT (80 μL) was added, and the incubation continued for another 2 h. After incubation at 37°C for 2 h, the absorbance (OD) at 570 nm was measured using an MB enzyme marker, and the IC_{50} value was calculated using *Graphpad Prism* 8.0. The inhibition rate of cell proliferation was calculated as follows: Inhibition rate= (ODcontrol group-ODexperimental group)/(ODcontrol group-ODblank group).

Declarations

Author Contribution

Baoxing Xie and Miaomiao Shi performed the experiments; Dan Tang performed the biology experiments ; Shan Yang and Yan Zeng analyzed the data; Lifei Niecontributed reagents; Chao Niu conceived and designed the study. All authors reviewed and approved the final version.

Acknowledgment

This research was supported by the Natural Science Foundation of Xinjiang Uygur Autonomous Region (2022D01A339, 2022D01A340); West Light Foundation of the Chinese Academy of Sciences (2023-XBQNXZ009); West Light Foundation of the Chinese Academy of Sciences (grant No. 2021-JCTD-001). Western Young Scholars Program of the Chinese Academy of Sciences (2021-XBQNXZ-009);

References

1. Boucherle B, Peuchmaur M, Boumendjel A, Haudecoeur R (2017) Occurrences, biosynthesis and properties of aurones as high-end evolutionary products. Phytochemistry 142:92–111. http://doi.org/10.1016/j.phytochem.2017.06.017
2. Li JQ, Xiao CJ, Li YM, Tian XY, Dong X, Jiang B (2020) Astrernestin, a novel aurone-phenylpropanoid adduct from the roots of Astragalus ernestii. Nat Prod Res 34:2894–2899. http://doi.org/10.1080/14786419.2019.1596101
3. Alsayari A, Muhsinah AB, Hassan MZ, Ahsan MJ, Alshehri JA, Begum N (2019) Aurone: A biologically attractive scaffold as anticancer agent. Eur J Med Chem 166:417–431.

http://doi.org/10.1016/j.ejmech.2019.01.078

4. Dokla EME, Abdel-Aziz AK, Milik SN, Mahmoud AH, Saadeldin MK, McPhillie MJ, Minucci S, Abouzid KAM (2021) Indolin-2-one derivatives as selective Aurora B kinase inhibitors targeting breast cancer. Bioorg Chem 117:105451. http://doi.org/10.1016/j.bioorg.2021.105451
5. Wu H, Zhao H, Lu T, Xie B, Niu C, Aisa HA (2023) Synthesis and Activity of Aurone and Indanone Derivatives. Med Chem 19:686–703. http://doi.org/10.2174/1573406419666230203105246
6. Sui G, Li T, Zhang B, Wang R, Hao H, Zhou W (2021) Recent advances on synthesis and biological activities of aurones. Bioorg Med Chem 29:115895. http://doi.org/10.1016/j.bmc.2020.115895
7. Chen Y, Yang M, Wang ZJ (2020) (Z)-7,4'-Dimethoxy-6-hydroxy-aurone-4-O-β-glucopyranoside mitigates retinal degeneration in Rd10 mouse model through inhibiting oxidative stress and inflammatory responses. Cutan Ocul Toxicol 39:36–42. http://doi.org/10.1080/15569527.2019.1685535
8. Saroha B, Kumar G, Arya P, Raghav N, Kumar S (2023) Some morpholine tethered novel aurones: Design, synthesis, biological, kinetic and molecular docking studies. Bioorg Chem 140:106805. http://doi.org/10.1016/j.bioorg.2023.106805
9. Chen S, Sun Q, Yao B, Ren Y (2024) The Molecular Mechanism of Aurora-B Regulating Kinetochore-Microtubule Attachment in Mitosis and Oocyte Meiosis. Cytogenet Genome Res 164:69–77. http://doi.org/10.1159/000540588
10. Ramkumar N, Patel JV, Anstatt J, Baum B (2021) Aurora B-dependent polarization of the cortical actomyosin network during mitotic exit. EMBO Rep 22:e52387. http://doi.org/10.15252/embr.202152387
11. Titova E, Shagieva G, Dugina V, Kopnin P (2023) The Role of Aurora B Kinase in Normal and Cancer Cells. Biochemistry 88:2054–2062. http://doi.org/10.1134/S0006297923120088
12. Ahmed A, Shamsi A, Mohammad T, Hasan GM, Islam A, Hassan MI (2021) Aurora B kinase: a potential drug target for cancer therapy. J Cancer Res Clin Oncol 147:2187–2198. http://doi.org/10.1007/s00432-021-03669-5
13. Lakkaniga NR, Wang Z, Xiao Y, Kharbanda A, Lan L, Li HY (2024) Revisiting Aurora Kinase B: A promising therapeutic target for cancer therapy. Med Res Rev 44:686–706. http://doi.org/10.1002/med.21994
14. Long S, Zhong Y, Liu J (2024) Aurora-B: a novel biomarker in the invasion and metastasis of osteosarcoma. Biomark Med 18:639–647. http://doi.org/10.1080/17520363.2024.2366160
15. He Y, Fu W, Du L, Yao H, Hua Z, Li J, Lin Z (2022) Discovery of a novel Aurora B inhibitor GSK650394 with potent anticancer and anti-*aspergillus fumigatus* dual efficacies *in vitro*. J Enzyme Inhib Med Chem 37:109–117. http://doi.org/doi: 10.1080/14756366.2021.1975693
16. Xu W, Kang C (2025) Fragment-Based Drug Design: From Then until Now, and Toward the Future. J Med Chem 68:5000–5004. http://doi.org/10.1021/acs.jmedchem.5c00424
17. Arús-Pous J, Patronov A, Bjerrum EJ, Tyrchan C, Reymond JL, Chen H, Engkvist O (2020) SMILES-based deep generative scaffold decorator for de-novo drug design. J Cheminform 12:38.

http://doi.org/10.1186/s13321-020-00441-8

18. Subbaiah MAM, Meanwell NA (2021) Bioisosteres of the Phenyl Ring: Recent Strategic Applications in Lead Optimization and Drug Design. J Med Chem 64:14046–14128. http://doi.org/10.1021/acs.jmedchem.1c01215
19. Jung Park Y, Jin Jung H, Jin Kim H, Soo Park H, Lee J, Yoon D, Kyung Kang M, Young Kim G, Ullah S, Kang D, Park Y, Chun P, Young Chung H, Ryong Moon H (2024) Thiazol-4(5H)-one analogs as potent tyrosinase inhibitors: Synthesis, tyrosinase inhibition, antimelanogenic effect, antioxidant activity, and in silico docking simulation. Bioorg Med Chem 98:117578. http://doi.org/10.1016/j.bmc.2023.117578
20. Wang S, Huo Y, Zhang J, Li L, Cao F, Song Y, Zhang Y, Yang K (2023) Design, synthesis, antitumor activity, and molecular dynamics simulations of novel sphingosine kinase 2 inhibitors. Bioorg Med Chem 93:117441. http://doi.org/10.1016/j.bmc.2023.117441

Scheme

Scheme 1 and 2 are available in the Supplementary Files section.

Figures

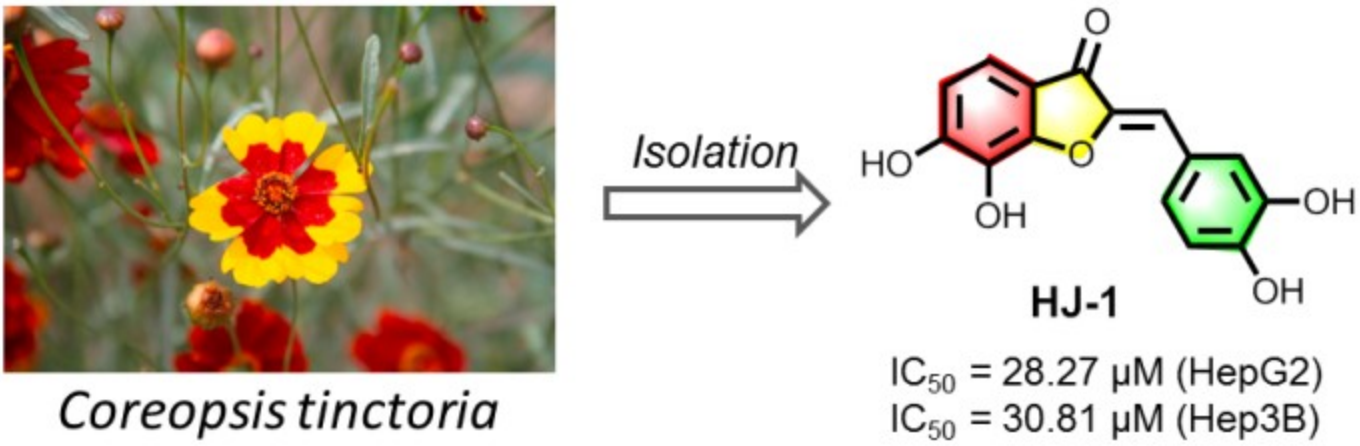

Figure 1

The aurone **HJ-1** from the *Coreopsis tinctoria*

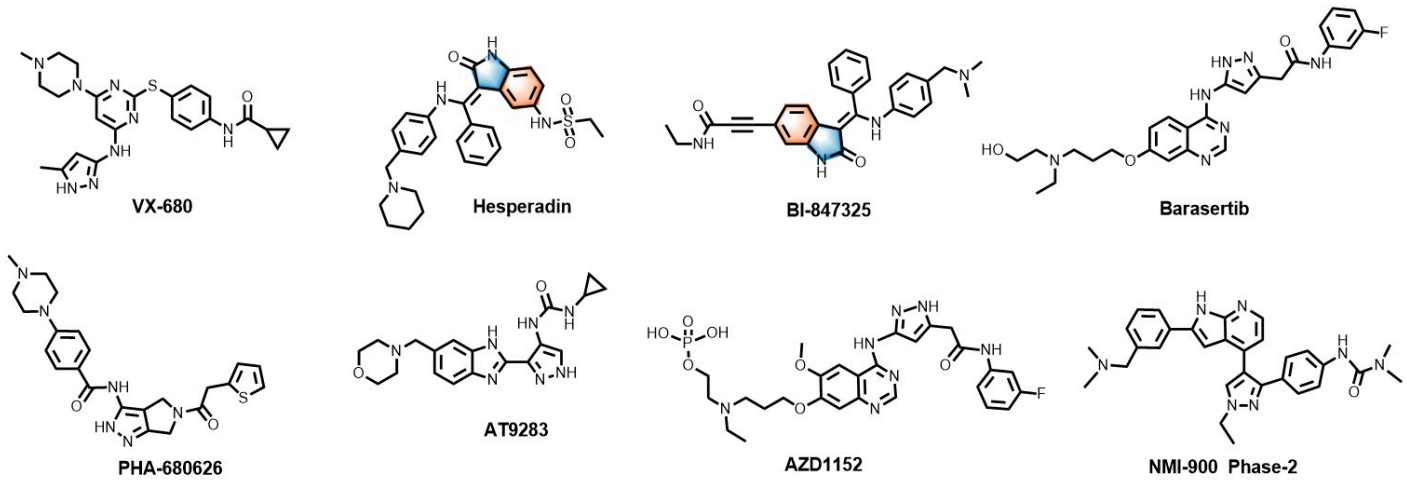

Figure 2

The structures of Aurora B inhibitors

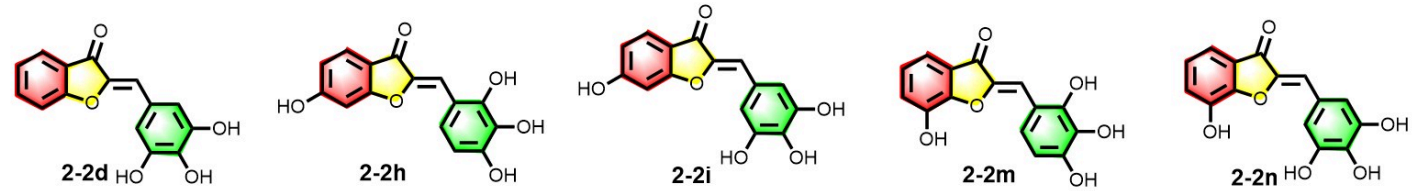

37.51% (Aurora A)
87.67% (Aurora B)

46.72% (Aurora A)
87.28% (Aurora B)

74.73% (Aurora A)
97.09% (Aurora B)

34.37% (Aurora A)
85.72% (Aurora B)

30.62% (Aurora A)
94.34% (Aurora B)

Figure 3

Synthesized aurones with high inhibiton and selectivity on Aurora B

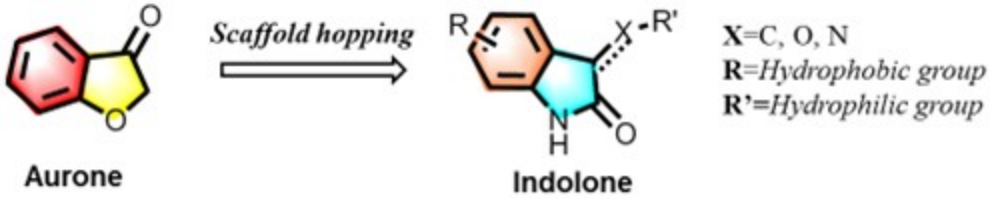

Figure 4

The scaffold hopping based on aurone

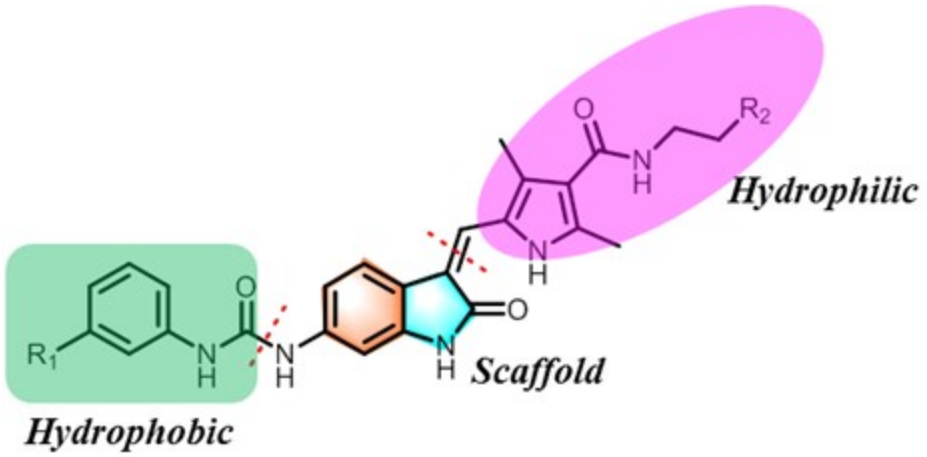

Figure 5

The structure of scaffold **3** identified by AIDD

Compounds	100 nM (%)	10 nM (%)	IC_{50} (nM)
3-17a	97.22	87.59	1.10
3-17b	94.52	65.89	40.24
3-17c	95.37	71.65	19.29
3-17d	97.65	82.10	1.52
3-17e	97.43	78.34	4.83
3-17f	90.41	59.65	40.67
3-17g	94.01	60.46	26.40
3-17h	95.50	76.56	10.37
3-17i	96.34	72.94	5.15
3-17j	94.73	62.83	35.13
3-17k	98.18	90.16	0.89
3-17l	87.69	47.41	77.90
3-17m	14.87	5.76	>500
3-17n	46.71	7.40	169.71
3-19	67.64	16.43	74.35
CCT241736	98.78	91.35	2.14

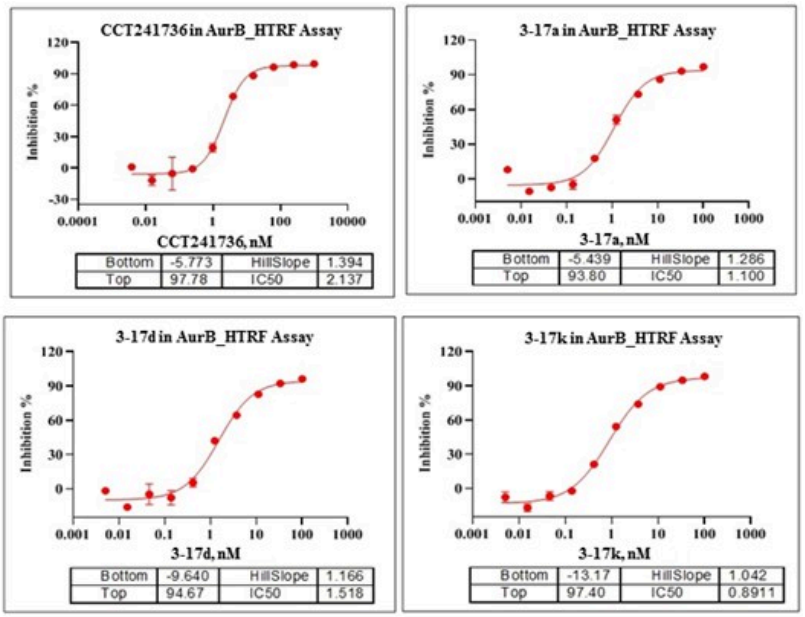

Figure 6

The inhibition rate and IC_{50} of **3-17a** to **3-17n** and **3-19** on Aurora B.

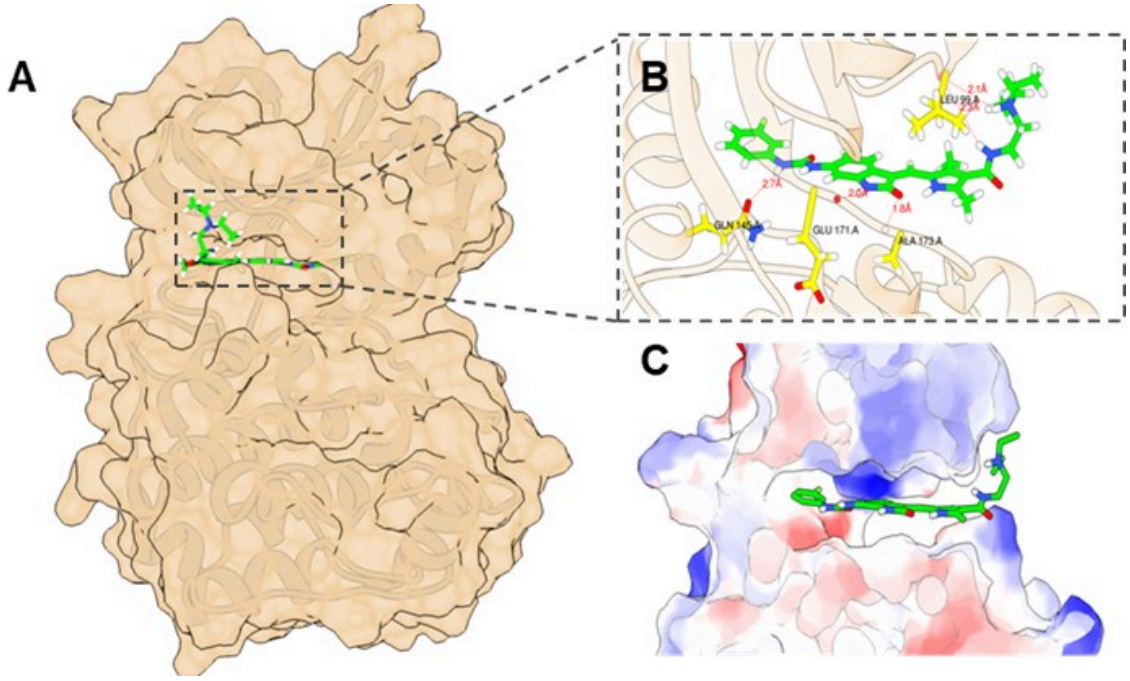

Figure 7

Molecular docking and electrostatic potential map of **3-17k** with Aurora B (PDB code: 5EYK). **A** and **B**: the binding mode of **3-17k** with Aurora B; **C**: the surface electrostatic potential map of the pocket.

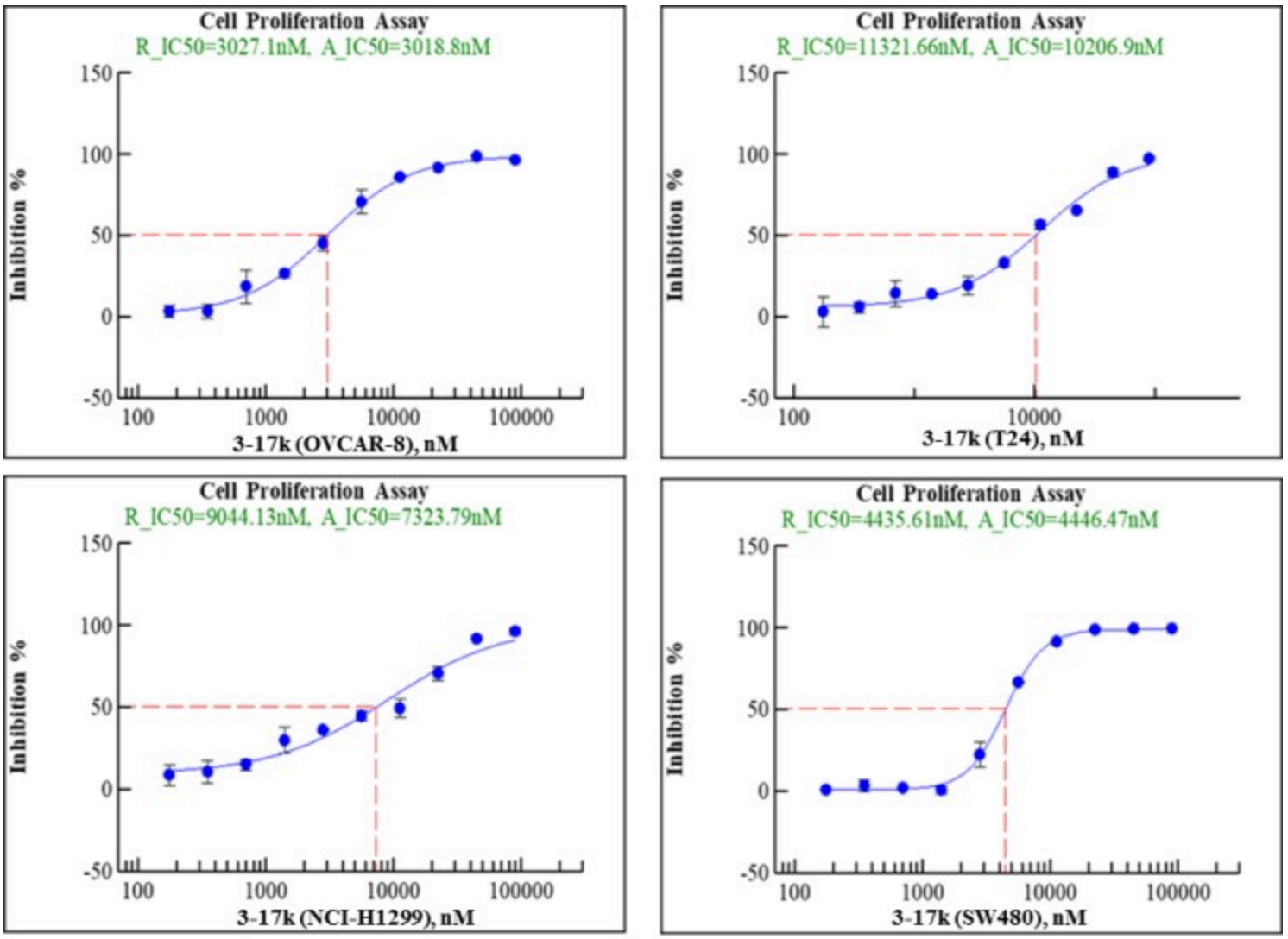

Figure 8

The IC_{50} of **3-17k** on Aurora B overexpression tumor cells

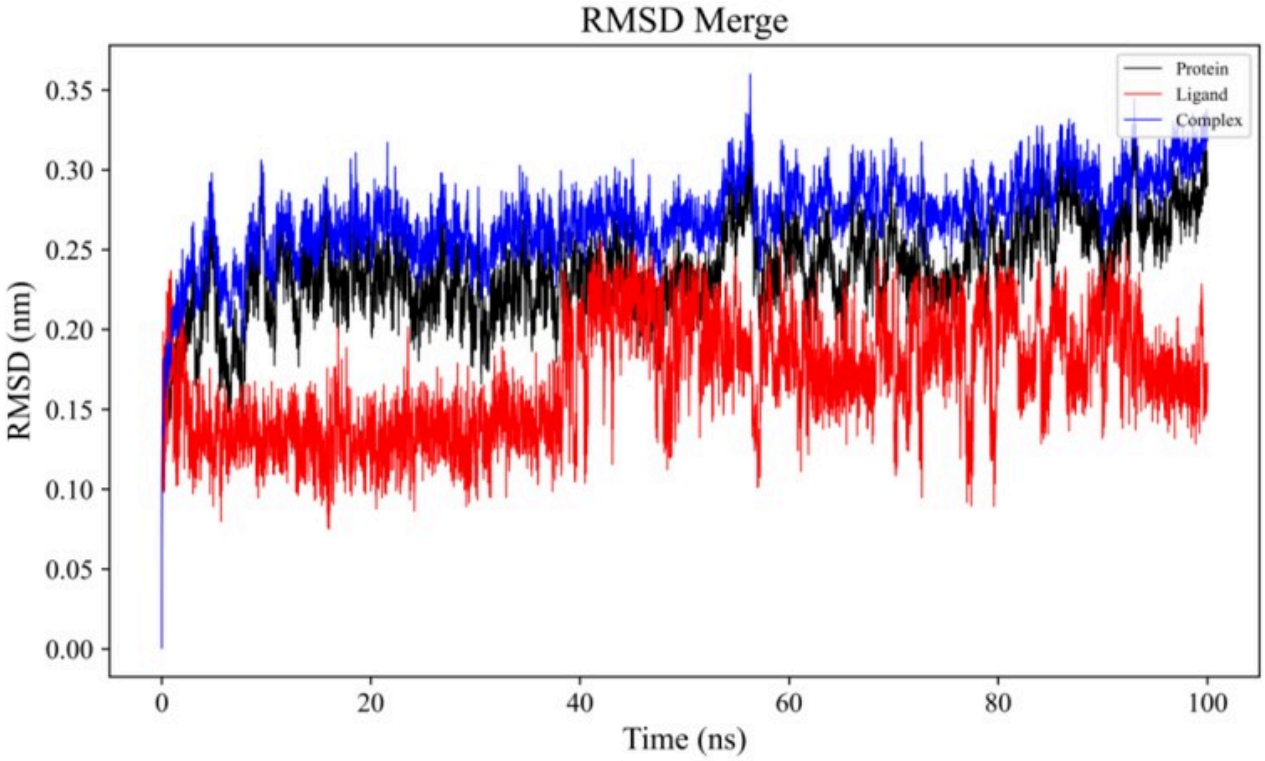

Figure 9

RMSD plot of **3-17k**_5EYK complex (blue), 5EYK apo (black), GHGT-17 (red) across 100 ns MD simulation trajectory

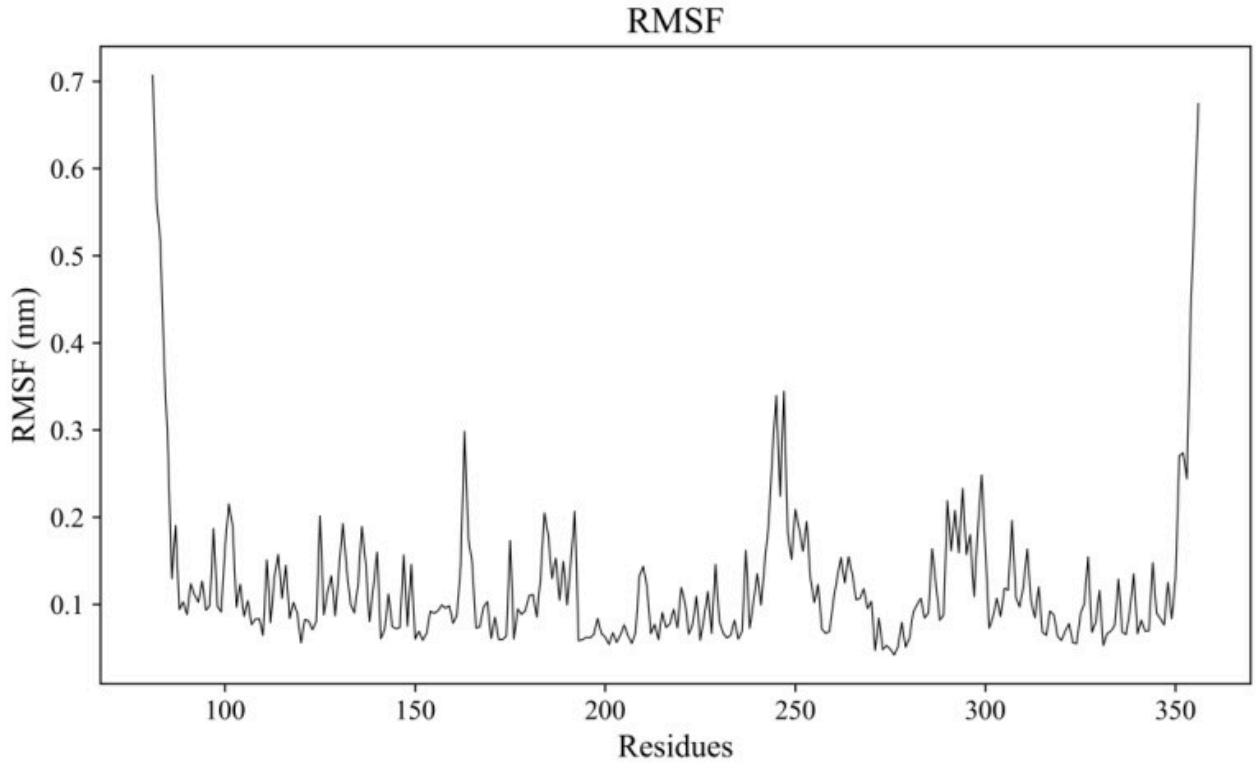

Figure 10

RMSF plot of complex across 100 ns MD simulation trajectory

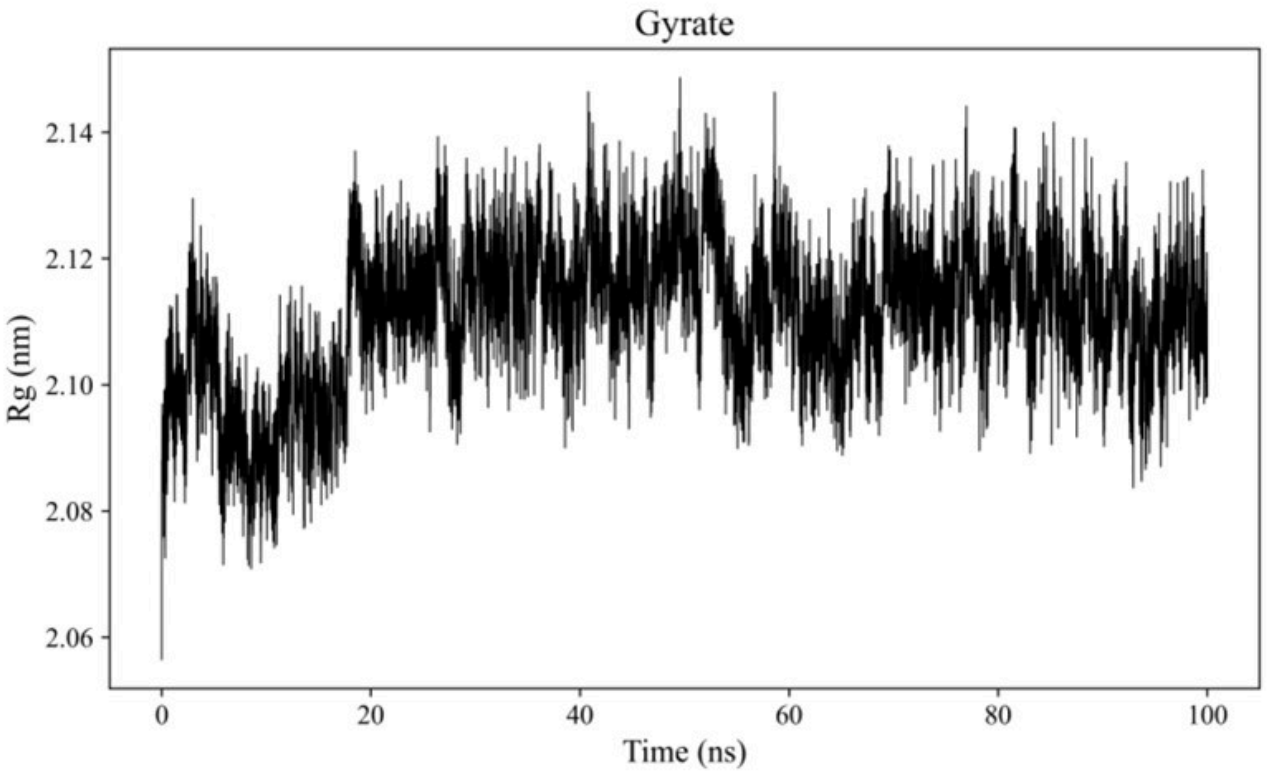

Figure 11

Radius of gyration plot of **3-17k**_5EYK complex across 100 ns MD simulation trajectory

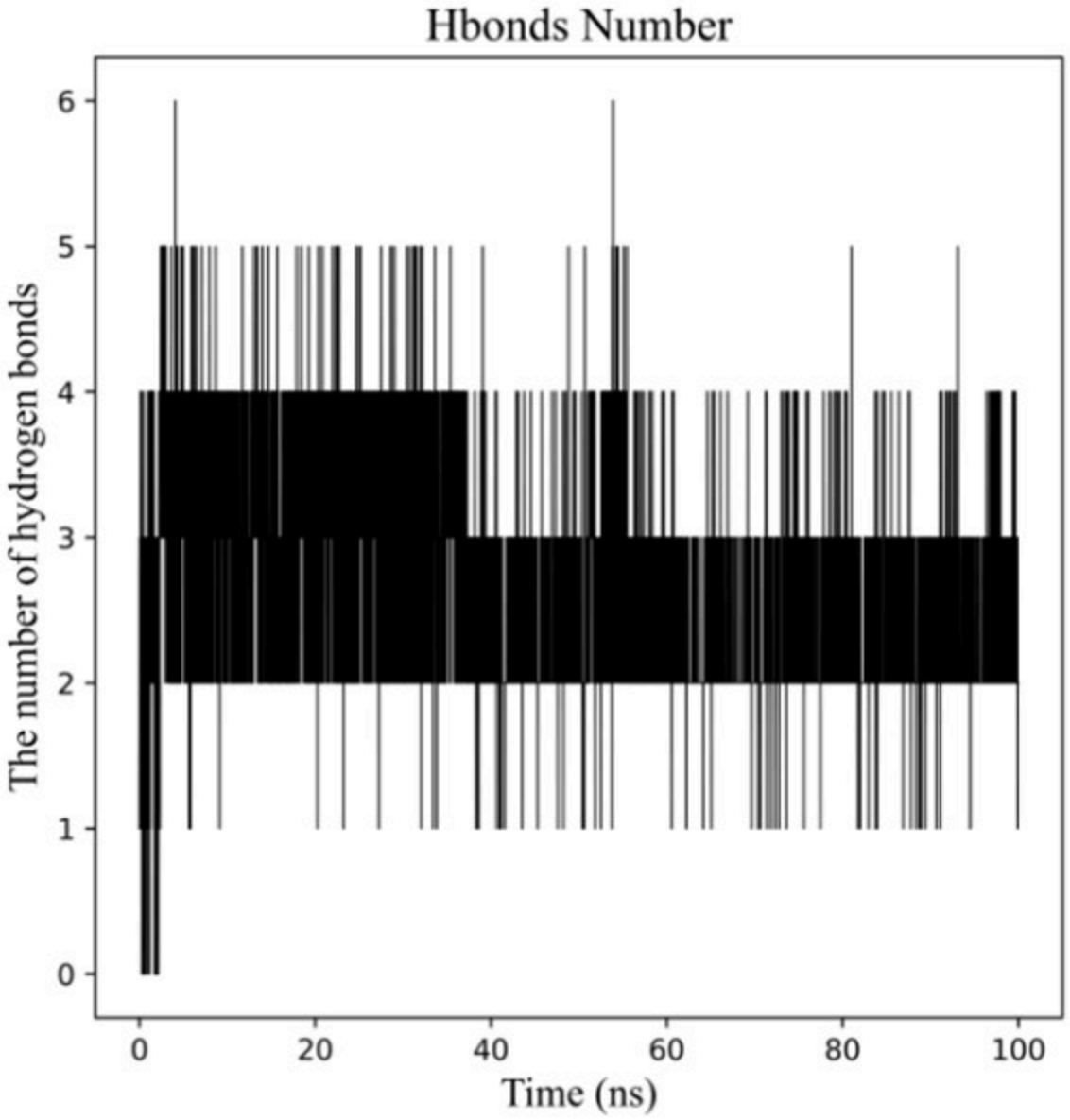

Figure 12

Number of H-bonds in **3-17k**_5EYK complex across 100 ns MD simulation trajectory

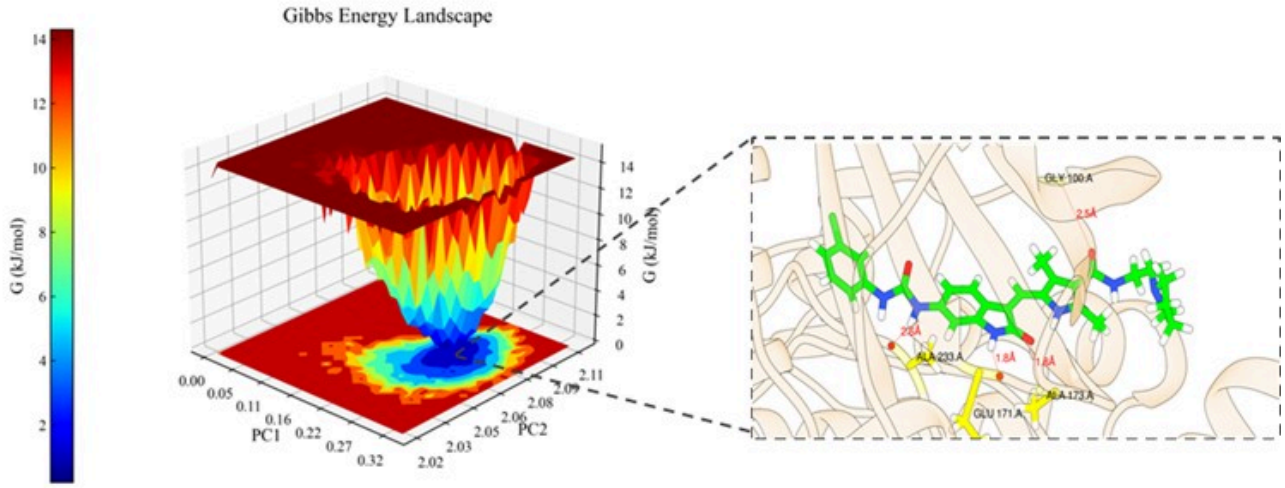

Figure 13

The FEL of **3-17k**_5EYK complex along PC1 and PC2.

(The conformations extracted from the minimum free-energy basins are next to FEL)

Supplementary Files

This is a list of supplementary files associated with this preprint. Click to download.

- SI.docx
- Scheme1.jpg
- Scheme2.jpg
- floatimage1.jpeg